EUDET-Report-2006-03

Measurements of radiation damages in the MIMOSA 5 pixel detector

Ł. Mączewski*and the EUDET JRA1 Collaboration†

September 8, 2006

Abstract

The MIMOSA 5 detector is a prototype of one of the proposed pixel detector concepts for the ILC vertex detector. High machine backgrounds expected in the ILC, especially due to e^+e^- pairs originating from beamstrahlung, require high radiation tolerance of the vertex detector modules. Results of the MIMOSA 5 detector irradiation with 9.4 MeV electrons are reported. Two MIMOSA 5 submatrices containing pixels with a "big" collecting diode, were exposed to two different fluences $\sim 3 \cdot 10^{12}$ e/cm^2 and $\sim 10^{13}$ e/cm^2. Pedestal and noise dependences on radiation dose and on temperature as well as the ADC-electron gain of the irradiated MIMOSA 5 are presented here.

*Warsaw University, Poland

†Bristol University (UK), CNRS-IRES, Institut de Recherches Subatomiques (Strasbourg, France), Commissariat a l'Energie Atomique, (Paris, France), Deutsches Elektronen-Synchrotron (Hamburg and Zeuthen, Germany), European Organisation for Nuclear Research (Geneva, Switzerland), High Energy Accelerator Research Organisation (Tsukuba, Japan), INFN Ferrara (Italy), INFN Milano (Italy), INFN Pavia (Italy), INFN Roma III (Italy), Laboratoire de Physique Subatomique et de Cosmologie (Grenoble, France), Max-Planck-Institut für Physik, Max-Planck-Gesellschaft (Munich, Germany), Radboud University (Nijmegen, Netherlands), Rutherford Appleton Laboratory (Oxfordshire, UK), The chancellor, Masters and Scholars of the University of Oxford (UK), Universität Bonn (Germany), Universität Mannheim (Germany), Université de Genéve (Switzerland), Warsaw University (Poland)

1 Requirements for a vertex detector for the ILC

The International Linear Collider (ILC) will be the next generation electron-positron accelerator based on a new acceleration technology which uses superconducting RF cavities. The ILC will allow high precision measurements in the clean environment of a lepton collider complementing the discoveries anticipated at the Large Hadron Collider (LHC).
Because of high luminosity ($2 \cdot 10^{34}$ cm^{-2}s^{-1}) and high energies in the ILC (at the beginning the energy in the center of mass will be 500 GeV upgradable to 1 TeV), large numbers of particles, containing b or c quarks will be produced. Such particles decay electro-weakly very close to the interaction point. In order to identify decay vertices of such short lived particles a very precise vertex detector is needed.
High granularity of the vertex detector will provide very good spatial resolution (it is expected to be better than 5 μm). Moreover, precise tracking of the low momentum particles requires detector plates to be only 0.1% X_0 thick.
High machine backgrounds, especially due to e^+e^- pairs originating from beamstrahlung, require high radiation tolerance of the detector. Electrons and positrons spiral in the solenoidal magnetic field and hit the detector layers several times. The biggest contribution to the radiation damage comes from $O(10)$ MeV electrons with trajectories confined to small radii by the magnetic field. The yearly ionisation dose caused by the low energy electron background is expected to be 50 krad and for the non-ionising damage expected fluence expressed in 1 MeV neutron equivalent fluence is around $2 \cdot 10^{10}$ cm^{-1}yr^{-1}. Particles from beamstrahlung have not only an impact on radiation damages but also on high occupancy of the detector (the innermost layer in the vertex detector needs to be read out 20 times per 50 μs).
One prototype of the proposed detector concepts for the ILC vertex detector is MIMOSA 5 (*Minimum Ionising MOS Active Pixel Sensor*) [1], made in CMOS technology (*Complementary Metal Oxide Semiconductor*). MIMOSA 5 is a monolithic active pixel sensor (MAPS) [2], i. e. the silicon that supports the R/O electronics is also the active material. MIMOSA 5 presents good spatial resolution and readout speed [3]. In this note irradiation tests of this device are reported.
Because most of the damages will be caused by $\sim$ 10 MeV electrons, irradiation with a $\sim$ 10 MeV electron beam were done at GSI in Darmstadt.

2 Radiation damages in silicon detectors

There are two main types of defects in semiconductor devices caused by radiation. These are: ($\imath$) atom displacements in the lattice and ($\imath\imath$) ionisation damages [2]. Atom displacements cause changes in the semiconductor bulk. These kind of damages are called bulk damages. Atom displacements are also responsible for the creation of trapped charges and interface defects and these effects are known as surface damages. Ionising radiation affects mostly properties of the readout electronics.
All the above effects lead to an increase of the leakage current, translating into an in-

crease of pedestals and noises as well as reduction of the collected charge in a physical signal due to charge trapping and a decrease of carriers mobility and their life time.

- **Displacement damages**
  We can distinguish two types of displacement defects: point defects and cluster defects. Point defects are mostly created by electromagnetic radiation of low energy electrons and X-rays. Cluster defects are caused by massive, high energy particles. If an interacting particle has sufficient energy to displace an atom from the lattice in the crystal, an interstitial-vacancy pair is created. In case of massive, high energy particles many such pairs are created (cluster defects). In general a great part of the interstitials and vacancies recombine and repair initial defects but some of them migrate, interact with impurities and form irreversible defects.
  Point defects produce new energy levels in the band gap. These energy levels can act as acceptors, donors or charge traps. Displacement damages cause increase of capture, generation and recombination rates of non equilibrium charge carriers. They also affect the internal electric field by changing effective doping concentration. Macroscopic manifestations of displacement effects are: increase of the leakage current, charge collection losses, changes in capacitance and material resistivity.
  Irradiation with heavy particles often creates large non uniformities in the dark current spatial distribution in the detector.

- **Ionisation damages**
  Another kind of radiation damage is that caused by charged particles. If a charged particle or a photon has sufficient energy, an e-h pair is produced in the medium. Many electrons and holes recombine in the initial phase but some of them drift and diffuse far from the point where they were produced and get blocked in some region, giving rise to the presence of charged zones. Ionisation damages are mainly concentrated at interfaces between different materials (e.g. $Si - SiO_2$) and cause an increase of the number of the interface traps which produce new energy levels. The latter act like additional acceptors, donors or charge traps. Charge carriers generated by incident particles get blocked in trapping centers and are released with some delay. Moreover increase of energy levels in a band gap causes an increase of the leakage current.
  Front-end electronics suffers a lot from ionisation damages. Absolute value of threshold voltages, in both NMOS and PMOS transistors increase due to creation of new interface traps and additional energy levels.

3 Description of the MIMOSA 5 detector

The MIMOSA 5 is the first real-scale MAPS pixel detector made in CMOS technology. The AMS 0.6 μm technology was used in the fabrication process of the MIMOSA 5. This technology enables generation of the 14.0 μm thick epitaxial layer (the epitaxial layer is the sensitive volume in the MAPS detectors [2]). The MIMOSA 5 consists

of 4 sub-matrices, 510 × 512 pixels each. Pixels in each sub-matrix have the same size: 17 × 17μm^2. Each pixel is equipped with a collecting diode. The only difference between sub-matrices arises from the different size of the collecting diodes. Pixels with "small" collecting diodes (3.1 × 3.1μm^2) are placed in two sub-matrices called T01 and B01 and pixels with "big" collecting diodes (4.9 × 4.9μm^2) are placed in other two sub-matrices called T02 and B02.

4 Irradiation setup in Darmstadt

MIMOSA 5 irradiation were done at GSI in Darmstadt with 9.4 MeV electrons (it was performed by Devis Contarato [3]). Sub-matrices with "big" collecting diodes were irradiated with two different fluences 3×10^{12} e/cm^2 and 10^{13} e/cm^2, equivalent to roughly 70 and 230 kGy, respectively.
The MIMOSA 5 chip was installed in a support frame and then irradiated with electrons (fig. 1(a)). In order to measure the beam profile a fluorescent screen was installed in place of the chip (fig. 1(b)). The fluorescent light from the screen was photographed by a CCD camera. The beam profile was measured with low electron beam current (when the beam current is low the fluorescent light should be a linear function of the absorbed electron dose).

(a) MIMOSA5 chip mounted in a support frame

(b) Fluorescent screen mounted in a support frame and a CCD camera watching on it

Figure 1: Experimental setup in Darmstadt.

In fig. 2(a) the picture from a CCD camera can be seen. The dark rectangle on this picture indicates the MIMOSA 5 sub-matrix. The transverse size of the beam was larger than the size of the MIMOSA 5 sub-matrices. Because of this even if the beam hits the center of one sub-matrix, the second matrix was absorbing electrons as well. This had to be taken into account during calculations of the entire dose absorbed by the different sub-matrices.
Fig. 2(b) presents the beam profile with a two dimensional function fitted (composition of a Gaussian and a Breit-Wigner). In fig. 2(c) and 2(d) projections of the beam profile

in x and y directions can be seen. This fit simplifies the beam profile and dose not take into account any of the fluctuations.

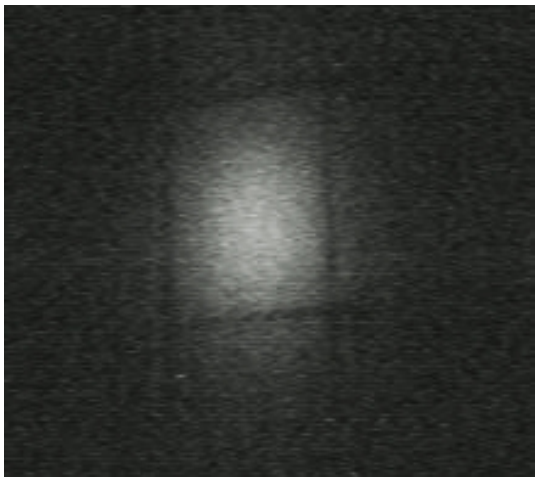

(a) Picture from the CCD camera

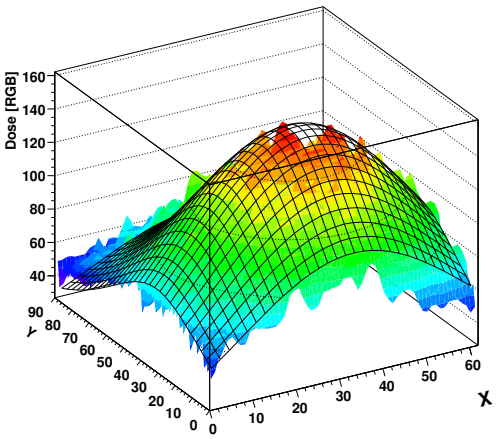

(b) Beam profile

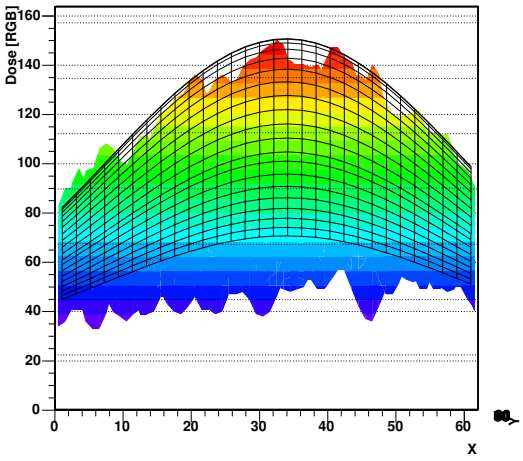

(c) x projection of the beam profile

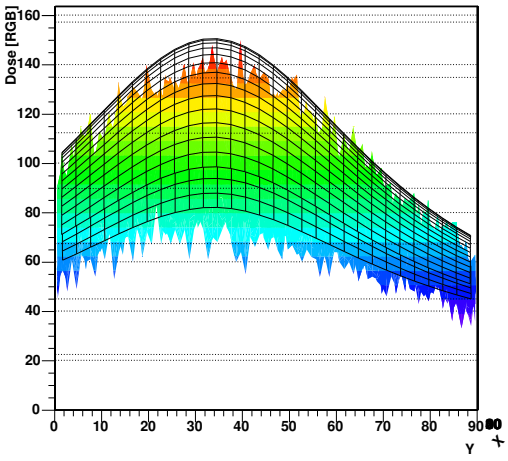

(d) y projection of the beam profile

Figure 2: Beam profile.

5 Pedestals and noises in irradiated MIMOSA 5 detectors

The raw signal is the sum of the pedestal (generated by electronic devices) and the physical signal left by a particle passing through the detector. The raw signal r_i^k in the k-th channel of the i-th event thus reads:

$$r_i^k = s_i^k + p_i^k, \tag{1}$$

where s_i^k is the physical signal and p_i^k is the pedestal.
To find the i-th channel pedestal estimator, raw data without physicals signal were selected ($r_i^k = p_i^k, s_i^k = 0$). The mean value of the pedestal was thus calculated:

$$< p_i >= \frac{1}{N}\sum_{i=1}^{N} r_i^k = \frac{1}{N}\sum_{i=1}^{N} p_i^k. \tag{2}$$

Noise of the i-th channel was defined as the variation of the pedestal p_i distribution and calculated according to:

$$< n_i >= \sqrt{\left(\frac{N}{N-1}\right)\left(\left(\frac{1}{N}\sum_{i=1}^{N} r_i^{k2}\right) - \left(\frac{1}{N}\sum_{i=1}^{N} r_i^k\right)^2\right)}. \tag{3}$$

In order to select raw data without physical signals a two step method was used. In the first step, the first N events from a given run were taken. These N events were divided into smaller buffers (5 events per buffer). The event with the highest raw value in the buffer was rejected and was not considered during the pedestal and the noise estimation (the efficiency of this method depends on the probability of finding two physical signals in the same buffer).
To subtract the physical signal from the raw data in the next events ($i > N$) estimators of the pedestal and the noise, calculated for the first N events, were used. If the absolute value of the difference between the raw signal and the estimated pedestal was five times lower than the estimated noise ($|r_i^k - p_i^k| < 5 \cdot n_i^k$), the signal was assumed to be free from the physical component and was used in the final estimation of the pedestal and the noise.

5.1 Pedestal and noise dependence on radiation dose

Pedestals and noises presented here and in subsection 5.2 were calculated using data taken without a source of particles. Because of this, there was no need for subtracting physical signals from raw data during calculations of pedestals and noises. Spatial distributions of pedestal and noise for both matrices are shown in fig. 3.

The shape of the pedestal spatial distributions on the detector surface corresponds to the beam profile used for irradiation. It can be said that there is a strong correlation

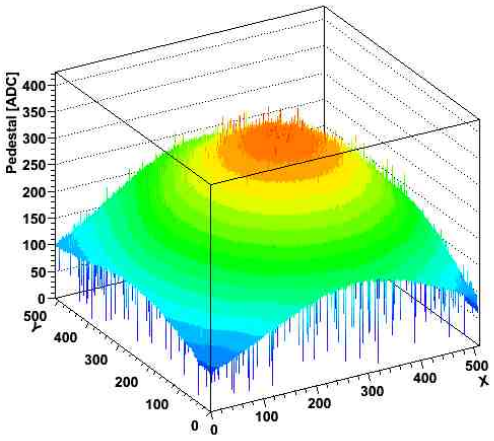

(a) Spatial distribution of pedestal (matrix T02)

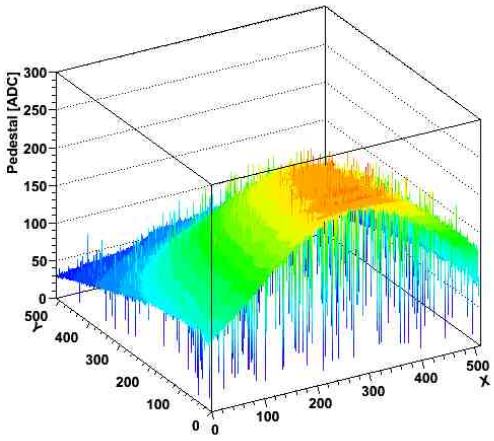

(b) Spatial distribution of pedestal (matrix B02)

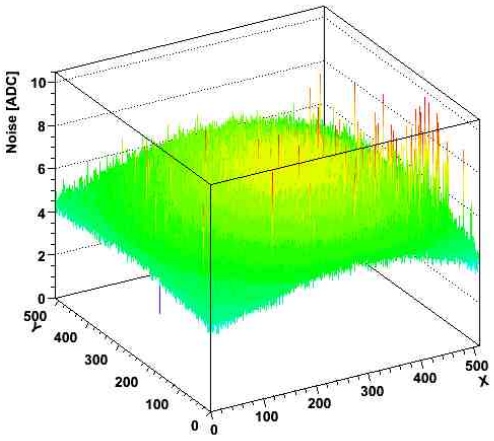

(c) Spatial distribution of noise (matrix T02)

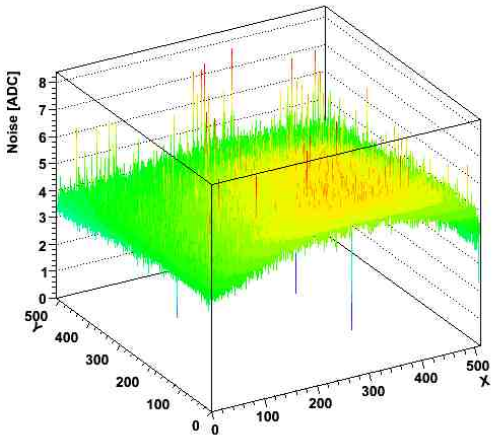

(d) Spatial distribution of noise (matrix B02)

Figure 3: Spatial distributions of pedestal and noise on the surface of tested detector (data taken in temperature $\sim -10^{\circ}$ C).

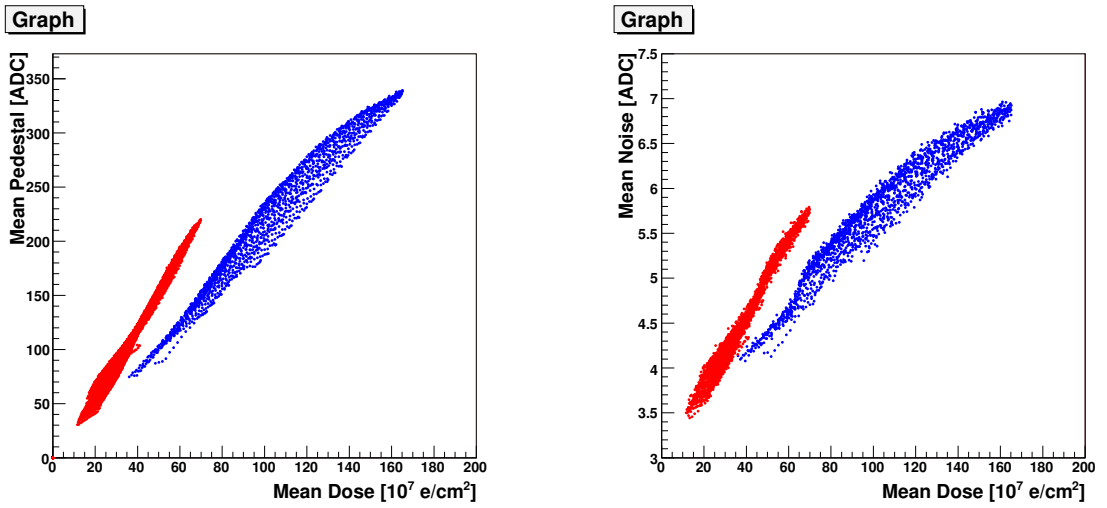

(a) Pedestal dependency on radiation dose

(b) Noise dependency on radiation dose

Figure 4: Pedestal and noise dependences on radiation dose. Red points correspond to matrix B02 and blue points to matrix T02.

between pedestal or noise and the dose absorbed by the detector. To find out how pedestal and noise depend on the radiation dose, the surface of the detector was divided into 4096 sub-areas (8 by 8 pixels each). In each sub-area a mean value of the pedestal or the noise was calculated and then compared to the beam profile. The results are shown in fig. 4.
It can be seen that pedestal and noise increases with the absorbed dose. Unfortunately the bad quality of the beam profile prevents establishing a function which precisely describes pedestal and noise dependence on the radiation dose. Pedestal should depend linearly on the radiation dose while noise like square root of the absorbed dose, but damages on the surface of the detector can influence these simple dependences.

5.2 Pedestal and noise dependence on temperature after irradiation

Pedestal is caused by a leakage current called the dark current which is proportional to the number of free charge carriers in a semiconductor. This number depends on temperature like $\sim T^2 \exp\left(E_g/k_B T\right)$ and pedestal should grow with the temperature in the same way. Noise is the result of fluctuations of the number of free charge carriers and it should grow with temperature like the square root of the charge carrier density $\sim T\sqrt{(\exp E_g/k_B T)}$.
To find the dependences of pedestal and noise on temperature, the surface of the B02 and the T02 matrix was again divided into 4096 sub-areas (8 by 8 pixels each). For each sub-area a mean pedestal, a mean noise and a variation of pedestal and noise were calculated. Dependence of the mean pedestal and the mean noise on temperature for one randomly chosen sub-area is presented in fig. 5 (errors represent variation of pedestals

or noises in the considered sub-area).

Measurements follow the theoretical predictions describing pedestal and noise dependence on temperature. The variation between theoretical predictions and data are probably caused by irradiation damages which instead of increasing the leakage current, decreased life time of charge carriers and increased the number of charge traps.
The latter source of irradiation damages could be responsible for the unnatural behaviour of the T02 matrix at low temperatures (matrix T02 was irradiated with higher dose). In fig. 6 the spatial distribution of mean pedestal and mean noise for the matrix T02

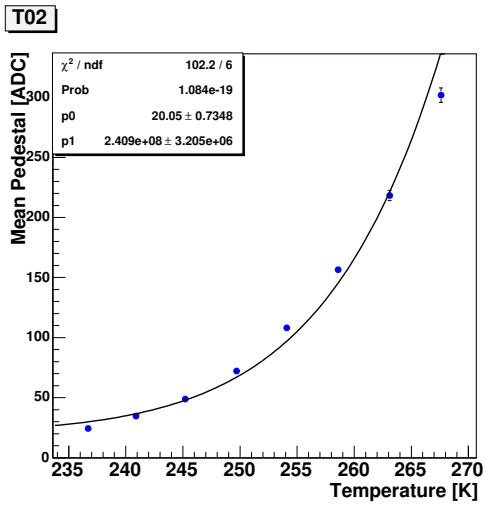

(a) Pedestal dependency on temperature (matrix T02)

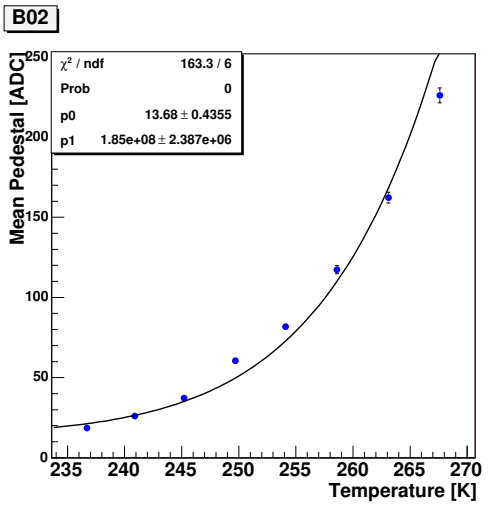

(b) Pedestal dependency on temperature (matrix B02)

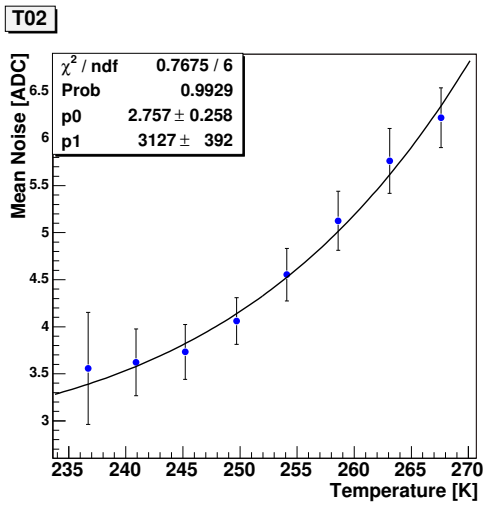

(c) Noise dependency on temperature (matrix T02)

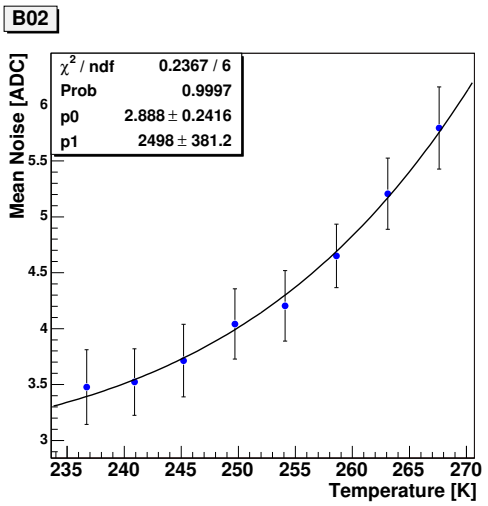

(d) Noise dependency on temperature (matrix B02)

Figure 5: Pedestal and noise dependences on temperature.

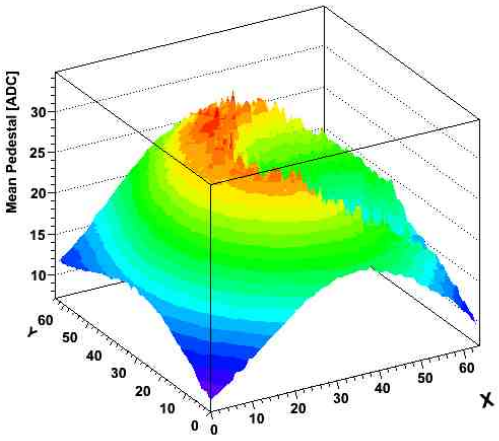

(a) Spatial distribution of mean pedestal (matrix T02)

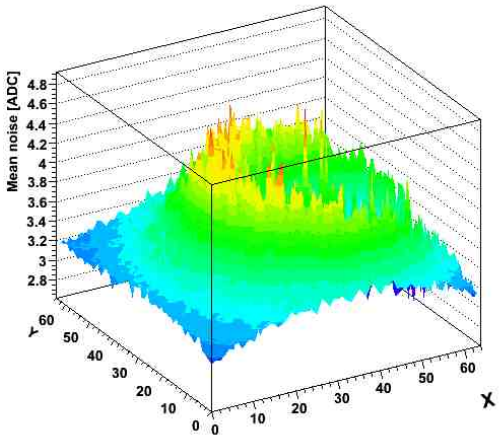

(b) Spatial distribution of mean noise (matrix T02)

Figure 6: Spatial distributions of mean pedestal and mean noise for matrix T02 at 243 K.

at 237 K are plotted. On the plots in fig. 6 one can distinguish the area in which mean pedestal and mean noise are much lower than one would expect.

6 Measurements with low energy X-rays

To find the ADC-electron gain of the MIMOSA 5 detector, a calibration with ^{55}Fe source was performed. A photon passing through the detector leaves charge which is then collected in pixels. If a photon interacts inside a field-free epitaxial layer, charge will spread to neighbouring pixels leading to the formation of clusters. Another possibility is that a photon interacts in a non-zero field region near the collecting diode. In such a case the entire generated charge is collected in a single pixel.
A pixel in which a major fraction of charge is collected is called the seed pixel and is situated closest to the point where the charged particle entered the detector. To find seed pixels, the following cuts were applied: the signal to noise ratio of the seed pixel has to be grater than 5 and the seed pixel has to collect the largest charge from all pixels in the cluster.
The charge distribution in seed pixels for both matrices is presented in fig. 7. The first peak, which dominates in fig. 7, is related to the incomplete charge collection. The second and the third peak (the latter hardly visible) are related to the emission lines of ^{55}Fe. Knowing that generation of an electron - hole pair in silicon requires 3.6 eV, photons of energy 5.9 keV and 6.49 keV will generate on average 1640 and 1804 electron pairs, respectively. Comparing the number of generated electrons and signals from the detector, expressed in ADC counts, the ADC-electron gain can be determined. For the matrix T02 before irradiation the gain was around 20.1 e/ADC counts and for the matrix

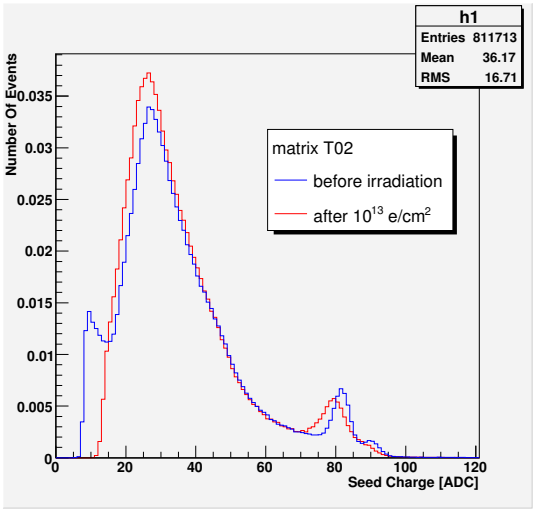

(a) Comparison of signals in seed pixel before and after irradiation for matrix T02

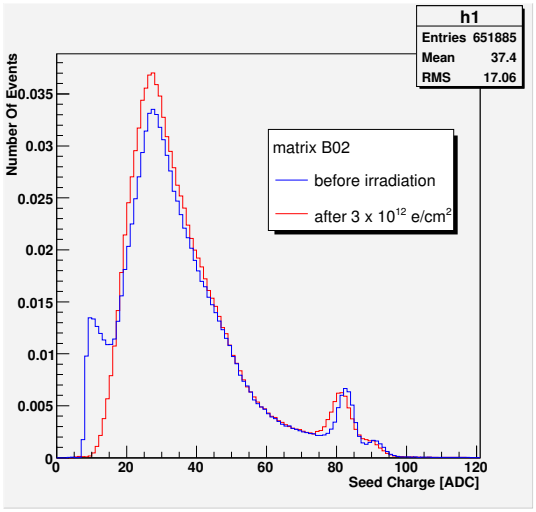

(b) Comparison of signals in seed pixel before and after irradiation for matrix B02

Figure 7: Comparison of signals in seed pixel before and after irradiation. The blue line corresponds to the measurements done before irradiation and the red one to the measurements done after irradiation.

B02 19.9 e/ADC counts.
Looking at fig. 7 one can see that after irradiation the peak related to the 5.9 keV photons is slightly shifted towards lower values. The ADC-electron gain changed after irradiation and the values for the matrix T02 and B02 are 20.7 e/ADC counts and 20.2 e/ADC counts, respectively. This effect is more significant for the matrix T02 which was exposed to the higher fluence. The reduction of the output signal after irradiation indicates charge collection losses. The radiation-induced trapping levels at the silicon-oxide interface and in the epitaxial layer are responsible for the charge collection losses in the silicon detectors.

7 Summary

The increases of pedestal and noise are the main effects observed after irradiation of the MIMOSA 5 detector at GSI in Darmstadt. Poor knowledge of the beam profile made it impossible to establish an accurate dependence of pedestal and noise on the absorbed dose. The beam profile should be better known for future measurements.
Measurements with the ^{55}Fe source show that irradiation of the MIMOSA 5 detector changed its charge collection properties. The additional radiation-induced energy levels at the silicon-oxide interface and in the epitaxial layer result in a reduction of the MIMOSA 5 output signal.

References

[1] C. Gilles, *Mimosa 5 test setup for DESY version 1*, LEPSI Strasbourg (2002).

[2] G. Deptuch, *Développement d'un capteur de nouvelle génération et son électronique intégrée pour les collisionneurs futurs*, Ph.D. Thesis, Université Louis Pasteur, Strasbourg (France), September 2002.

[3] D. Contaratto, *Silicon Detectors for Particle Tracking at Future High-Energy Physics Experiments*, Ph.D. Thesis, Hamburg University (Germany 2005).